



Cite this article: Kheradpezhoh E, Choy JMC, Daria VR, Arabzadeh E. 2017 TRPA1 expression and its functional activation in rodent cortex. *Open Biol.* **7**: 160314. <http://dx.doi.org/10.1098/rsob.160314>

Received: 22 November 2016

Accepted: 13 March 2017

Subject Area:

neuroscience/cellular biology

Keywords:

cortex, trpa1, layer 5 pyramidal neurons, optovin, photoswitching

Author for correspondence:

Ehsan Kheradpezhoh

e-mail: ehsan.kheradpezhoh@anu.edu.au

TRPA1 expression and its functional activation in rodent cortex

Ehsan Kheradpezhoh^{1,2}, Julian M. C. Choy¹, Vincent R. Daria¹
and Ehsan Arabzadeh^{1,2}

¹Ecdys Institute of Neuroscience, John Curtin School of Medical Research, and ²The Australian Research Council Centre of Excellence for Integrative Brain Research, Australian National University Node, Acton, Australian Capital Territory 2601, Australia

EK, 0000-0002-6155-4950

TRPA1 is a non-selective cation channel involved in pain sensation and neurogenic inflammation. Although TRPA1 is well established in a number of organs including the nervous system, its presence and function in the mammalian cortex remains unclear. Here, we demonstrate the expression of TRPA1 in rodent somatosensory cortex through immunostaining and investigate its functional activation by whole-cell electrophysiology, Ca²⁺ imaging and two-photon photoswitching. Application of TRPA1 agonist (AITC) and antagonist (HC-030031) produced significant modulation of activity in layer 5 (L5) pyramidal neurons in both rats and mice; AITC increased intracellular Ca²⁺ concentrations and depolarized neurons, and both effects were blocked by HC-030031. These modulations were absent in the TRPA1 knockout mice. Next, we used optovin, a reversible photoactive molecule, to activate TRPA1 in individual L5 neurons of rat cortex. Optical control of activity was established by applying a tightly focused femtosecond-pulsed laser to optovin-loaded neurons. Light application depolarized neurons ($n = 17$) with the maximal effect observed at $\lambda = 720$ nm. Involvement of TRPA1 was further confirmed by repeating the experiment in the presence of HC-030031, which diminished the light modulation. These results demonstrate the presence of TRPA1 in L5 pyramidal neurons and introduce a highly specific approach to further understand its functional significance.

1. Introduction

Transient receptor potential ankyrin 1 (TRPA1) is a member of the ancient superfamily of transient receptor potential (TRP) channels that are generally involved in pain, thermal and chemical sensation [1,2]. TRPA1 is a non-selective cation channel, exhibits high structural similarity to TRP vanilloid 1 (TRPV1), and contains the longest N-terminal among all known TRP channels in vertebrates [1,3,4]. The N-terminal contains 14–18 ankyrin repeat domains which represent the binding site for TRPA1 activators including non-specific irritants and Ca²⁺ [1,3–6]. TRPA1 is broadly expressed throughout the body including brain, heart, small intestine, lung, bladder, joints and skeletal muscles [7–15]. As a mechanosensor, TRPA1 is expressed in the peripheral sensory pathways and in the inner ear [16–18]. TRPA1 is prominently present in the nociceptive neurons of dorsal root ganglia (DRG) and the trigeminal ganglia [19], and is activated by a range of irritants including mustard oil, acrolein, formalin and 4-hydroxynonenal [1,3,20–22]. In the central nervous system, TRPA1 is studied in the hippocampus [14] and the supraoptic nucleus of the brain stem [7,23].

Despite the widespread agreement about the role of TRPA1 in pain sensation and neurogenic inflammation, our knowledge of its expression and function in the cerebral cortex remains minimal. TRPA1 loses its functionality in excised membrane patches due to several biophysical and cellular regulatory sites [4,24,25] which have been confirmed by the recent discovery of TRPA1's

molecular structure [26]. Non-specific agonists have been used to study TRPA1 function including pungent molecules extracted from wasabi, garlic and cinnamon [20,27–29] and synthetic compounds such as unsaturated aldehydes, trinitrophenol and 2-aminoethoxydiphenyl-borate (2-APB) [4,24,25]. Although known TRPA1 agonists often activate other TRP channels (but see [30]), there are several specific TRPA1 antagonists including AP-18 [31], Chembridge-5861528 [32,33], A-967079 [34] and HC-030031 [35]. Recently, optovin—a small synthetic molecule—was used to specifically target TRPA1 channels and to produce motor behaviours in wild-type zebrafish [36]. Optovin contains an α,β -unsaturated rhodanine system, an olefin-like compound that reacts with the cysteine residue of TRPA1. Besides its TRPA1-binding site, optovin contains a rhodopsin-photoactive site; application of violet light (387 nm) reversibly photoswitches optovin which in turn activates TRPA1 channels [36]. The optovin photoswitching thus allows activation of TRPA1 at high spatial and temporal precision in order to study its function in brain tissue.

Here, we first demonstrate the presence of TRPA1 in rodent somatosensory cortex with immunostaining, calcium imaging and whole-cell recording. We then use optovin photoswitching to probe TRPA1 function in cortical neurons at high temporal resolution. Rather than single-photon photoswitching with violet light, we achieve a highly localized excitation method via nonlinear two-photon photoswitching. Optovin photoswitching thus allows us to specifically gate TRPA1 channels and to activate individual layer 5 (L5) pyramidal neurons. Two-photon excitation uses a near-infrared (NIR) femtosecond (fs) pulsed laser, which penetrates deeper into the brain tissue.

2. Material and methods

2.1. Preparation of brain slices

Coronal brain slices (300 μm) were prepared from 28–35 day old male Wistar rats, wild-type C57Bl/6J mice and TRPA1 knockout (TRPA1-KO) mice; the brain was sliced with a vibratome (DSK Microslicer[®]) in ice-cold oxygenated artificial cerebrospinal fluid (aCSF) containing (in mM): 1.25 NaH_2PO_4 , 1.0 MgCl_2 , 125.0 NaCl , 2.5 KCl , 2.0 CaCl_2 , 25.0 NaHCO_3 and 10.0 glucose. Slices were then incubated at 34°C for 30 min in a holding chamber containing carbogen (5% CO_2 /95% O_2) bubbled aCSF and then kept at room temperature in the same chamber.

2.2. Two-photon Ca^{2+} imaging

Neurons were loaded with the Ca^{2+} indicator by incubating the slices in carbogen-bubbled aCSF containing 5 μM Cal-520 acetoxymethyl ester (Cal-520 AM; AAT Bioquest, Sunnyvale, CA, USA) at room temperature for 45 min. After three episodes of 5 min washing with carbogen-bubbled aCSF, the slices were transferred to the chamber for fluorescence imaging. Slices were continuously perfused with 36 \pm 1°C carbogen-bubbled aCSF containing (in mM): 1.25 NaH_2PO_4 , 1.0 MgCl_2 , 125.0 NaCl , 2.5 KCl , 2.0 CaCl_2 , 25.0 NaHCO_3 and 25 glucose at the rate of 2–3 ml min^{-1} . Ca^{2+} imaging was performed using a two-photon microscope (Thorlabs Inc., Newton, NJ, USA) controlled by THORIMAGE OCT software. The brain slice was illuminated with a Ti:Sapphire fs-pulsed laser (Chameleon, Coherent Inc., Santa Clara, CA, USA) tuned at 810 nm. The

laser was focused through a 16 \times water-immersion objective lens (0.8NA, Nikon) onto the tissue and Ca^{2+} transients were obtained from neuronal populations at a resolution of 512 \times 512 pixels (sampling rate, 10 Hz). The change in fluorescence activity ($\Delta F/F$) was quantified after importing images into IMAGEJ software (National Institutes of Health, USA) and by manual selection of the regions of interest (ROIs) around the neuronal cell bodies.

2.3. Whole-cell electrophysiology

After transferring the slices to the recording chamber, visualized whole-cell patch-clamp recording was performed on L5 pyramidal neurons in the somatosensory cortex using differential interference contrast (DIC) video microscopy. Slices were continuously perfused with 36 \pm 1°C carbogen-bubbled aCSF containing (in mM): 1.25 NaH_2PO_4 , 1.0 MgCl_2 , 125.0 NaCl , 2.5 KCl , 2.0 CaCl_2 , 25.0 NaHCO_3 and 25 glucose at the rate of 2–3 ml min^{-1} . The neuronal viability and functionality were tested by recording the membrane's voltage and action potentials in response to a depolarizing current pulse in the current clamp mode. The internal solution contained (in mM): K-gluconate, 115; KCl , 20; HEPES, 10; phosphocreatine, 10; Mg-ATP , 4; Na-GTP , 0.3 and biocytin, 0.25%. The pH of the internal solution was titrated with 1M KOH to a final pH of 7.3 and the osmolarity adjusted to 305 mOsm l^{-1} with water or sucrose. The recording pipette contained 0.25% biocytin (Sigma-Aldrich Co. LLC., Rockville, MD, USA) for morphological reconstruction and optovin (Tocris Bioscience, Bristol, UK). Recording of the membrane currents was made in whole-cell voltage clamp mode using a MultiClamp 700B amplifier (Molecular Devices, Sunnyvale, CA, USA). Bridge balance and capacitance neutralization were carefully adjusted and checked for stability. A series of current steps (duration 500 ms, amplitudes ranging from –80 to 500–2000 pA in increments of 40 pA) was applied to identify neuronal firing patterns. Action potentials were recorded in whole-cell current clamp mode using the same amplifier. Only cells with a stable resting membrane potential from the start of the patch were chosen for recording. Voltage or current traces were filtered at 10 kHz and digitized at 20–50 kHz by an ITC-18 interface (HEKA Instruments Inc., Holliston, MA, USA) under the control of AXOGRAPH software (Axograph Scientific, Berkeley, CA, USA). To modulate TRPA1 activity, we applied AITC (TRPA1 agonist, 1 mM) and HC-030031 (TRPA1 antagonist, 10 μM) through the bath solution. Although lower concentrations of AITC were effective in activation of TRPA1 in transfected HEK cells [35], we selected a high concentration (1 mM) based on previous experiments on native cells [11,37–39]. Similarly we used a concentration of 10 μM for HC-030031, compatible with previous studies [35].

2.4. Two-photon activation of optovin-loaded neurons

Pyramidal neurons were filled with 0.1 mM Alexa-488 and imaged using a custom-built two-photon microscope [39] that allowed for visualizing the sample via an upright DIC image (Olympus BX50WI) to facilitate patching of neurons in 300 μm thick brain slices. In DIC imaging mode, the dichroic mirror (DM) above the objective lens allowed NIR light ($\lambda > 900$ nm) to pass through and focus onto a charge-coupled device (CCD) camera (Dage-MTI IR-1000EX). In

the two-photon mode, a set of xy galvanometer (GM) scanning mirrors scanned the incident laser for raster imaging and for random positioning of focal stimulation of the neurons. The microscope used a 40× objective lens (Zeiss 1.0NA). Custom software developed in LABVIEW (National Instruments) controlled the acquisition of three-dimensional (3D) images, and the laser intensities via a polarizing beam splitter and a half-wave plate on a motorized rotation mount. During optovin activation, the change in membrane potential was monitored in whole-cell current clamp. Two separate lasers were used, one for imaging (Coherent Mira 900 pumped with 12 W Verdi G) and one for two-photon photoswitching of optovin (Coherent Chameleon, wavelength tuneable from $\lambda = 700$ to 1100 nm). Two-photon imaging was acquired by setting the laser at $\lambda = 850$ nm and 5–10 mW average power. For two-photon photoswitching, the laser was set to $\lambda = 700$ to 800 nm at 10–20 mW average power. After breaking into the cell, we waited for a minimum of 3 min to allow optovin perfusion, before applying the laser. TRPA1 activation was limited to the recorded neuron because the excitation was localized within the diameter of the laser focus (approx. 1 μm) [40]. We activated TRPA1 along the dendritic shaft close to the soma. To identify the optimal stimulation parameters, we applied the following six wavelengths: $\lambda = 700, 720, 730, 760, 780$ and 800 nm. Every trial contained a 100-ms light stimulation with an inter-trial interval of 1300 ms. Different wavelengths and intensities were applied in blocks of 20 trials. To allow recovery from stimulation, and for the membrane potential to return to baseline, we applied a 1-min pause between consecutive blocks. These blocks were interleaved and repeated in a pseudorandom order to produce a total of 60 trials per each wavelength/intensity combination.

2.5. Immunohistochemistry

At the completion of the experiment, the brain slices were fixed in 4% paraformaldehyde in phosphate buffered saline (PBS) at 4°C. After fixation, the slices were rehydrated gradually by step-wise incubation in 10 to 30% sucrose in PBS (w/v). After rehydration, the slides were sectioned with a Leica CM1580 cryostat at 60 μm thickness and penetrated using PBS containing 1% Triton-X (v/v) for 4–5 h at room temperature under continuous shaking. The slides were washed three times with PBS at room temperature. To visualize the biocytin loaded neurons, the slices were incubated with streptavidin Alexa Fluor® 488 conjugate (Thermo Fisher Scientific, Waltham, MA, USA) overnight at 4°C on a shaker. To investigate the TRPA1 expression, the slices were incubated first with rabbit anti-TRPA1 primary antibody (AB58844, Abcam, Cambridge, UK) overnight at 4°C on a shaker, washed three times, and then incubated with either goat (488) or donkey (555) anti-rabbit IgG Alexa Fluor® secondary antibody (Abcam, Cambridge, UK). To stain the nuclei of cortical cells, the slices were briefly (approx. 10 min) incubated with 4',6-diamidino-2'-phenylindole dihydrochloride (DAPI) (Sigma-Aldrich Co. LLC., Rockville, MD, USA) at room temperature on a shaker. After washing, the slices were mounted on glass slides using PDX New (Merck, Darmstadt, Germany) and dried. Images were captured with a Nikon A1 confocal microscope. Laser-generated excitation wavelengths of 405, 488 and 555 nm were used to detect DAPI (nuclei), Alexa Fluor® 488 (biocytin and TRPA1) and Alexa Fluor® 555 (TRPA1), respectively. The IMAGES were then processed by

IMAGEJ (JACoP Plugin) and colocalization scatter plots were created in MATLAB (Mathworks, Natick, MA, USA).

3. Results

3.1. Cortical expression of TRPA1

In the first step, we investigated the expression of TRPA1 in the rat somatosensory cortex. We prepared coronal brain slices from male Wistar rats aged 28–35 days and determined TRPA1 expression by application of TRPA1-specific antibodies (figure 1a). We discovered TRPA1 expression in neurons across all cortical layers (figure 1b). Beyond cortical neurons, the immunostaining results also revealed expression of TRPA1 in hippocampal neurons (H in figure 1b) and cortical vessels (figure 1d) as previously reported [7,26,41]. The level of TRPA1 expression in cortical neurons seems comparable with that of the hippocampal neurons.

To further examine the expression of TRPA1 in neurons, we loaded individual L5 pyramidal cells with biocytin using patch pipettes and quantified the colocalization of TRPA1 and biocytin using confocal microscopy (figure 2a,b). Across 156 non-overlapping z-stack images captured from three reconstructed neurons, we found that colocalization was in the range of 0.19–0.67 (Pearson's correlation coefficient) with a mean \pm s.e.m. of 0.42 ± 0.13 (figure 2c,d). A mirror rotation of the biocytin (green) images significantly reduced the correlation values (paired *t*-test, $p < 0.0001$) to 0.02–0.09 at all z-stack images indicating that TRPA1 expression followed the outline of the neuron. A critical next step was to verify whether TRPA1 could be functionally activated in cortical neurons. We investigated this question with electrophysiological and Ca^{2+} imaging experiments conducted in the presence and absence of TRPA1 agonist and antagonist.

3.2. TRPA1 modulation of the membrane potential

To examine the physiological effect of TRPA1 activation on neurons, we performed *in vitro* whole-cell recording of L5 pyramidal cells (figure 2a) and measured the changes in membrane potential (V_m) in the presence of TRPA1 agonist (allyl isothiocyanate, AITC) and TRPA1 antagonist (HC-030031). Application of 1 mM AITC increased V_m significantly (depolarization, $n = 8$, $p < 0.0001$). AITC is a well-recognized TRPA1 agonist gating the channel by reversible covalent binding to the N-terminal [42]; however, it is not selective to TRPA1 only and can exert its effect through non-specific binding to other TRP channels [30,43]. In order to see whether the effect observed in figure 2e was through activation of TRPA1 channels, in a subset of neurons ($n = 5$) we followed the application of AITC with 10 μM HC-030031, a highly selective TRPA1 antagonist. After a few minutes of exposure to HC-030031, V_m returned towards its baseline levels ($n = 5$, $p < 0.0001$, figure 2f). In another subset of neurons ($n = 3$), the application of AITC was followed by more than 20 min of washing with aCSF (figure 2f). This allowed us to discriminate between the antagonistic activity of HC-030031 and a non-specific wash-out of AITC. The return to baseline V_m was only observed in the HC-030031 group with no decline in V_m for the prolonged wash (paired *t*-test, $p < 0.001$).

Next, we asked if these changes in membrane potential also corresponded to changes in intracellular Ca^{2+} . To

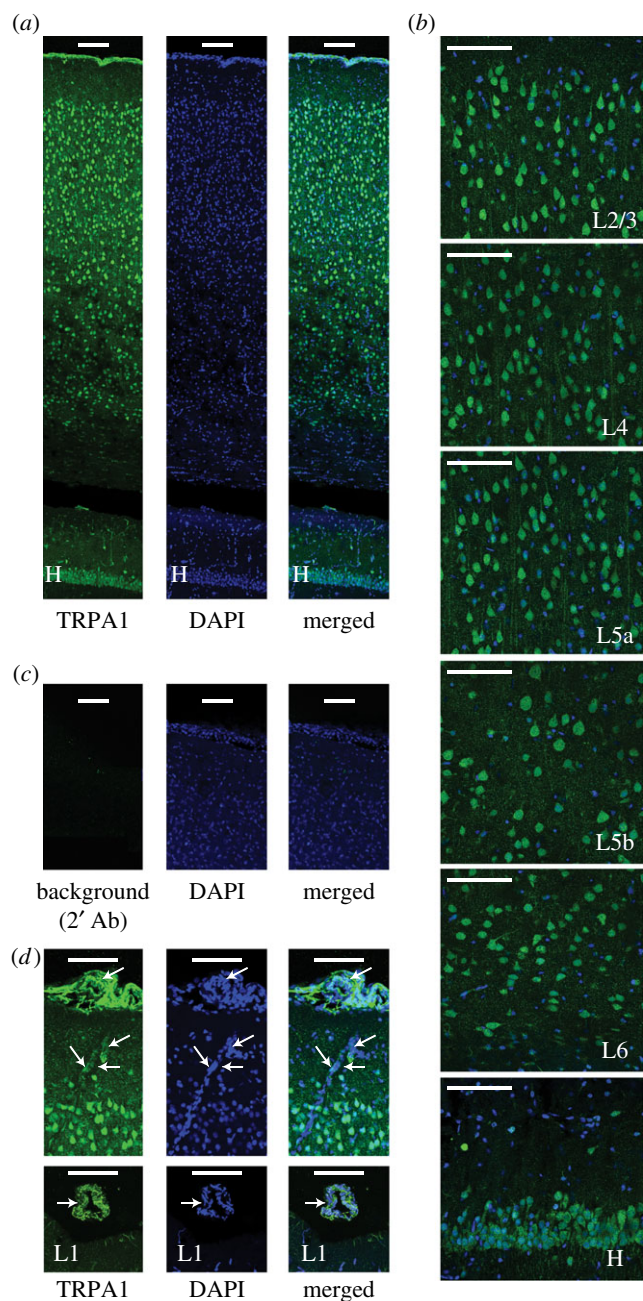


Figure 1. TRPA1 expression in the rat cortex. (a) Confocal images of a cortical slice (coronal section) capture anti-TRPA1 antibody (green) merged with nuclear staining with DAPI (blue). (b) TRPA1 expression in neurons across all cortical layers (L2/3, L4, L5a, L5b and L6) and in the hippocampus (H). (c) Incubation of the brain sections with secondary antibody alone (2' Ab) shows minimal non-specific binding of the secondary antibody to the brain slices. (d) TRPA1 is prominently expressed in cortical blood vessels (arrows). Scale bar, 100 μm in all panels.

examine this we employed two-photon Ca^{2+} imaging, which further allowed us to test the effect of TRPA1 activation on a population of neurons.

3.3. TRPA1 modulation of neuronal Ca^{2+}

We conducted two-photon Ca^{2+} imaging on brain slices prepared from 28–35-day-old Wistar rats and measured the relative changes in the cytosolic Ca^{2+} concentration ($[\text{Ca}^{2+}]_c$) of L5 pyramidal neurons. As TRPA1 channels are more permeable to Ca^{2+} than other cations [44], activation of TRPA1 by agonists is expected to produce a measurable increase in neuronal $[\text{Ca}^{2+}]_c$. We quantified the relative changes in

fluorescence ($\Delta F/F$) after application of AITC and HC-030031. Introducing AITC in the bath solution significantly increased $\Delta F/F$ indicating a rise in neuronal $[\text{Ca}^{2+}]_c$ (paired *t*-test, $p < 0.001$). After replacing AITC with 10 μM HC-030031, the neuronal $[\text{Ca}^{2+}]_c$ returned to its baseline values (figure 3).

3.4. Modulations are absent in the TRPA1-KO mice

In earlier results, whole-cell electrophysiology and Ca^{2+} imaging revealed significant modulation of activity in L5 pyramidal neurons by TRPA1 agonist and antagonist. A powerful method to verify that the observed functional modulations were indeed through the TRPA1 channel is to employ knockout models that specifically lack this channel. A TRPA1 knockout mouse does exist, where the exons required for proper function of TRPA1 were deleted [45]. The results up to now have all reported experiments conducted on rats. We therefore repeated the electrophysiology and Ca^{2+} imaging in the TRPA1-KO as well as the control wild-type C57Bl/6 J mice.

The procedures for slice preparation, electrophysiology and imaging were similar to those used on rats. The electrophysiology and Ca^{2+} imaging demonstrated the lack of functional modulation by the agonist and antagonist in the TRPA1-KO while replicating the earlier findings in the wild-type mice (figure 4). *In vitro* whole-cell recording of L5 pyramidal cells revealed systematic modulations of V_m in the presence of AITC and HC-030031 in the wild-type (red data points in figure 4*b,c*) but not in the TRPA1-KO (green data points in figure 4*b,c*). The V_m modulations in wild-type were qualitatively similar to those observed earlier in rats. Figure 4*d* illustrates the relative changes in fluorescence ($\Delta F/F$) after application of AITC and HC-030031. As observed earlier in rat cortex, for the wild-type mouse cortex introducing AITC in the bath solution increased $\Delta F/F$, indicating a rise in neuronal $[\text{Ca}^{2+}]_c$. After replacing AITC with 10 μM HC-030031, the neuronal $[\text{Ca}^{2+}]_c$ returned to its baseline values (red traces in figure 4*d,e*). Compared with the wild-type, the modulation in the neuronal $[\text{Ca}^{2+}]_c$ was minimal in the TRPA1-KO and did not return to baseline after application of HC-030031. There was a significant difference in AITC modulation across the population of 153 cells imaged from the wild-type, and 156 cells imaged from the TRPA1-KO (paired *t*-test, $p < 0.001$).

3.5. Two-photon photoswitching of optovin-loaded neurons

Altogether, the immunostaining, electrophysiological and Ca^{2+} imaging results support the idea that L5 pyramidal neurons exhibit functional TRPA1 channels. However, our results so far do not exclude the possibility of indirect activation of neurons by gating TRPA1 channels present in the cortical tissue including in glial cells and blood vessels. In other words, the observed changes in V_m and $[\text{Ca}^{2+}]_c$ may not be mediated by direct activation of TRPA1 channels of the recorded neuron. To rule out the possibility of an indirect TRPA1 activation in the cortex, we need a method where activation can be restricted to a single neuron. Targeted light application to photoswitch optovin in single cells provides this possibility.

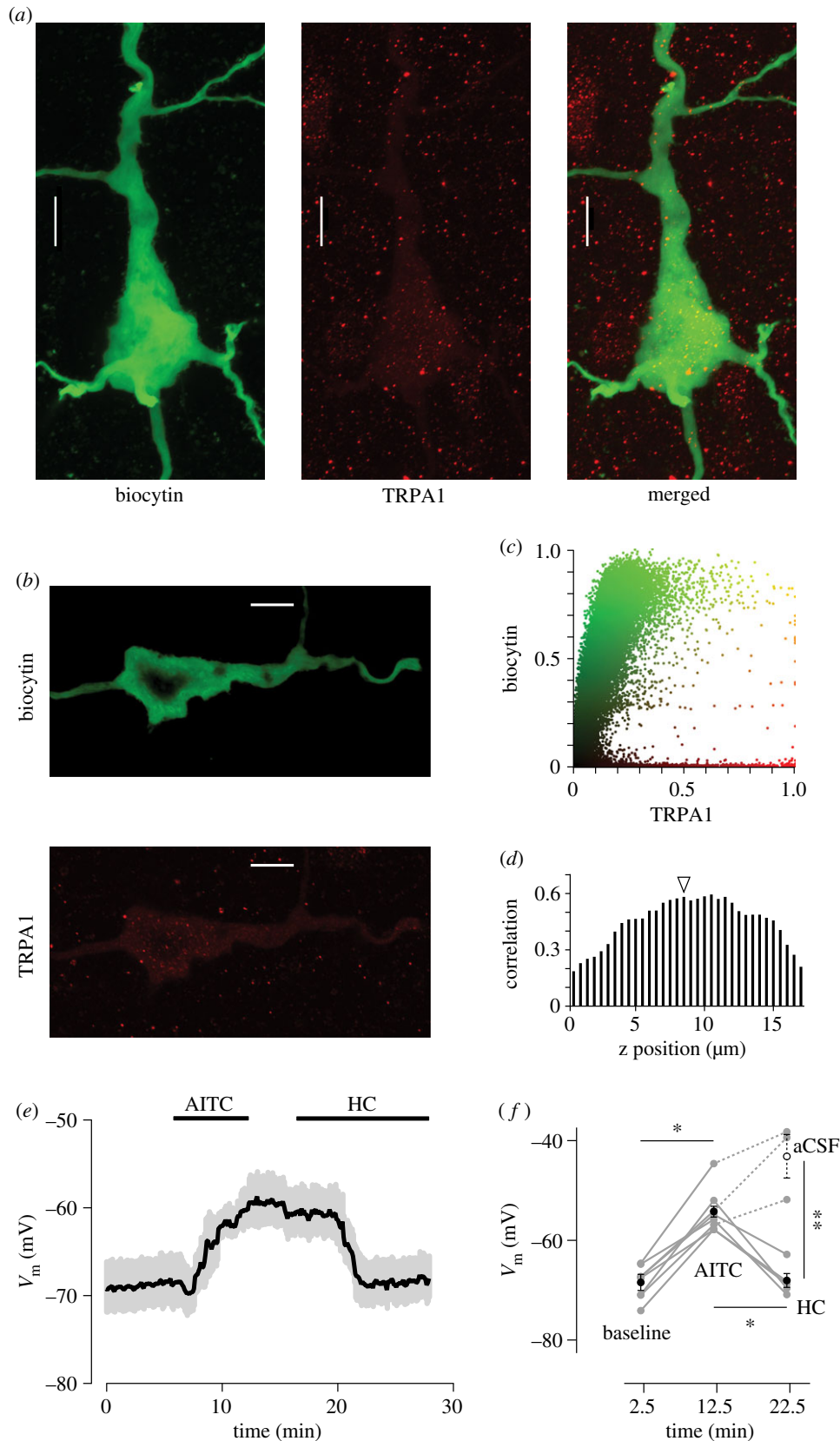


Figure 2. TRPA1 expression in individual L5 pyramidal neurons. (a) Z-stacked confocal images of an L5 pyramidal neuron loaded with biocytin (green) and visualized by tagged-streptavidin (left panel). TRPA1 expression reveals the outline of the neuron (middle panel). The merged image shows the overlap between biocytin and TRPA1 (right panel). A total of 33 z-stacks at 0.5- μm spacing were combined to generate each panel. Scale bar, 10 μm . (b) A single z-stack image of the neuron shown in (a). (c) The scatterplot shows the normalized fluorescent values at every pixel. Every dot is coloured by combining the relative fluorescent intensities in green (biocytin) and red (TRPA1) fluorochromes. The scales are normalized from 0–1 for green and red fluorochromes. (d) Pearson's correlation coefficient values (correlation) at each z position (0–17 μm) of the neuron shown in (a). Z-stack images were acquired through confocal microscopy with 0.1 μm thickness at 0.5 μm intervals. The arrow indicates the correlation value for the section shown in (b). (e) Whole-cell recording of L5 pyramidal neurons reveal depolarization with TRPA1 agonist AITC. The shaded area indicates s.e.m. of V_m across neurons ($n = 5$). By replacing AITC with specific TRPA1 antagonist HC-030031 (HC), the membrane potential returned to its baseline values (hyperpolarized). (f) V_m plotted individually for the eight neurons (grey circles) at each critical time point: at baseline (baseline, 2.5 min, $n = 8$); after application of agonist (AITC, 12.5 min, $n = 8$); after application of antagonist (HC, 22.5 min, $n = 5$); and after prolonged wash (aCSF, 22.5 min, $n = 3$). Black circles with s.e.m. show mean values at each time point. * $p < 0.001$, ** $p = 0.025$.

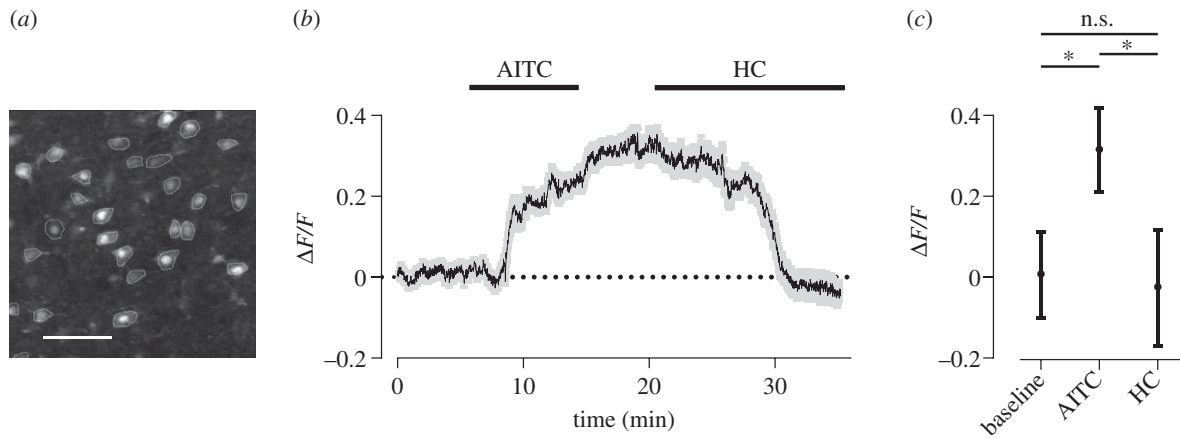


Figure 3. TRPA1 activation increases intracellular calcium. (a) The two-photon image shows 27 L5 cells loaded with Cal-520 in one imaging session. The regions of interest were manually selected at the margin of the cells. Scale bar, 50 μm . (b) Five minutes after the onset of imaging, AITC was applied to the bath, followed by washing and then by application of HC-030031 (HC). The grey shaded area indicates s.e.m. of $\Delta F/F$ across neurons ($n = 79$) recorded in three imaging experiments. (c) $\Delta F/F$ measured at three time points after the onset of imaging: 2.5 min (baseline), 12.5 min (AITC) and 32.5 min (HC). $\Delta F/F$ is measured over a 1 s duration for each cell and averaged across cells ($n = 79$). Error bars indicate s.d. of $\Delta F/F$ across neurons. * $p < 0.001$, n.s., $p > 0.05$.

Optovin is a photoactive molecule that gates TRPA1 after it is photoswitched by violet light [36]. The specificity for TRPA1 is supported by the finding that optovin photoswitching was significantly abolished in DRG neurons harvested from TRPA1 knockout mice [36]. Here, we replaced the violet light with an NIR fs-pulsed laser for a less scattered targeting. Localized photoswitching allows us to limit activation to TRPA1 channels in an optovin-loaded neuron (figure 5a). To achieve this, we performed *in vitro* whole-cell recording of L5 pyramidal neurons from rat somatosensory cortex using an internal solution containing optovin. We then applied the NIR fs-pulsed laser, 1 μm in diameter (see [40]), to the dendritic shaft of the patched neuron. The internal application of optovin along with the focused light ensures direct activation of TRPA1 channels restricted to the recorded neuron. The sample neuron shown in figure 5b was loaded with 3 μM optovin and excited at its dendritic shaft (the laser was focused at the location marked with the arrow). We found that 100 ms application of NIR fs-pulsed laser at wavelengths in the range $\lambda = 700\text{--}800$ nm modulated the neuron's membrane potential. Figure 5c shows the membrane potential averaged across 20 repetitions of laser stimulation at each wavelength. Minimal depolarization was induced at the longest wavelength ($\lambda = 800$ nm). The depolarization gradually increased with decreasing wavelength and peaked at $\lambda = 720$ nm. Further decrease in the wavelength below $\lambda = 720$ nm reduced the degree of depolarization. The depolarization also depended on the laser power (figure 5d): increasing the intensity of the two-photon excitation beam from 14 mW (blue) to 20 mW (red) produced a significant upward shift in the neuronal response. These findings were replicated across neurons: light activation was observed for all recorded L5 pyramidal neurons ($n = 17$) with the maximum neuronal response detected consistently at $\lambda = 720$ nm (figure 5e). As a control experiment, we applied the same protocol in the absence of optovin and found no effects of laser stimulation (see below). In the next step, we further investigate the optimal parameters for optovin photoswitching.

3.6. Optimal parameters for light activation of optovin

We first determined how light activation depended on the cellular concentration of optovin. By increasing the

concentration of optovin, ΔV_m increased significantly and even resulted in firing action potentials in some of the recorded cells. Figure 6a illustrates the firing profile of an example L5 pyramidal neuron along with its morphological reconstruction; this neuron was loaded with 20 μM optovin. Here, two-photon photoswitching with NIR fs-pulsed laser ($\lambda = 720$ nm, 20 mW, for 100 ms) produced reliable firing of action potentials across all trials. For this neuron, the membrane potential before and after each stimulation block remained stable at approximately -70 mV. There was however high trial-to-trial variability in the V_m during the stimulation block (figure 6a). To quantify how the excitation depended on the presence of optovin and its concentration, neurons were loaded with 0, 1, 3, 5, 10 and 20 μM optovin. As optovin is introduced through the internal pipette solution, only a single concentration could be applied to each neuron. A total of 30 neurons were recorded ($n = 5$ for each concentration). Changes in membrane potential were measured after removing any action potentials. Figure 6b illustrates how the degree of light-induced depolarization increased with optovin concentration. The dose–response curve is plotted on a logarithmic axis and does not show the recordings that were performed in the absence of optovin; in the absence of optovin laser stimulation at $\lambda = 720$ nm wavelength and with maximum light power (20 mW) did not produce any depolarization in the recorded neurons ($n = 5$; before and after light paired *t*-test $p > 0.2$).

3.7. Optovin photoswitching activates neurons through TRPA1 channels

Finally, to confirm that optovin activated these neurons via its specific interaction with TRPA1, we repeated the whole-cell recordings in the presence or absence of the selective TRPA1 blocker HC-030031 (10 μM). The neuronal response was significantly reduced in the presence of the blocker (figure 7a, paired *t*-test $p < 0.0001$) and this was true for all recorded neurons loaded at three different concentrations of optovin (figure 7b, $n = 6$, all *p*-values < 0.02).

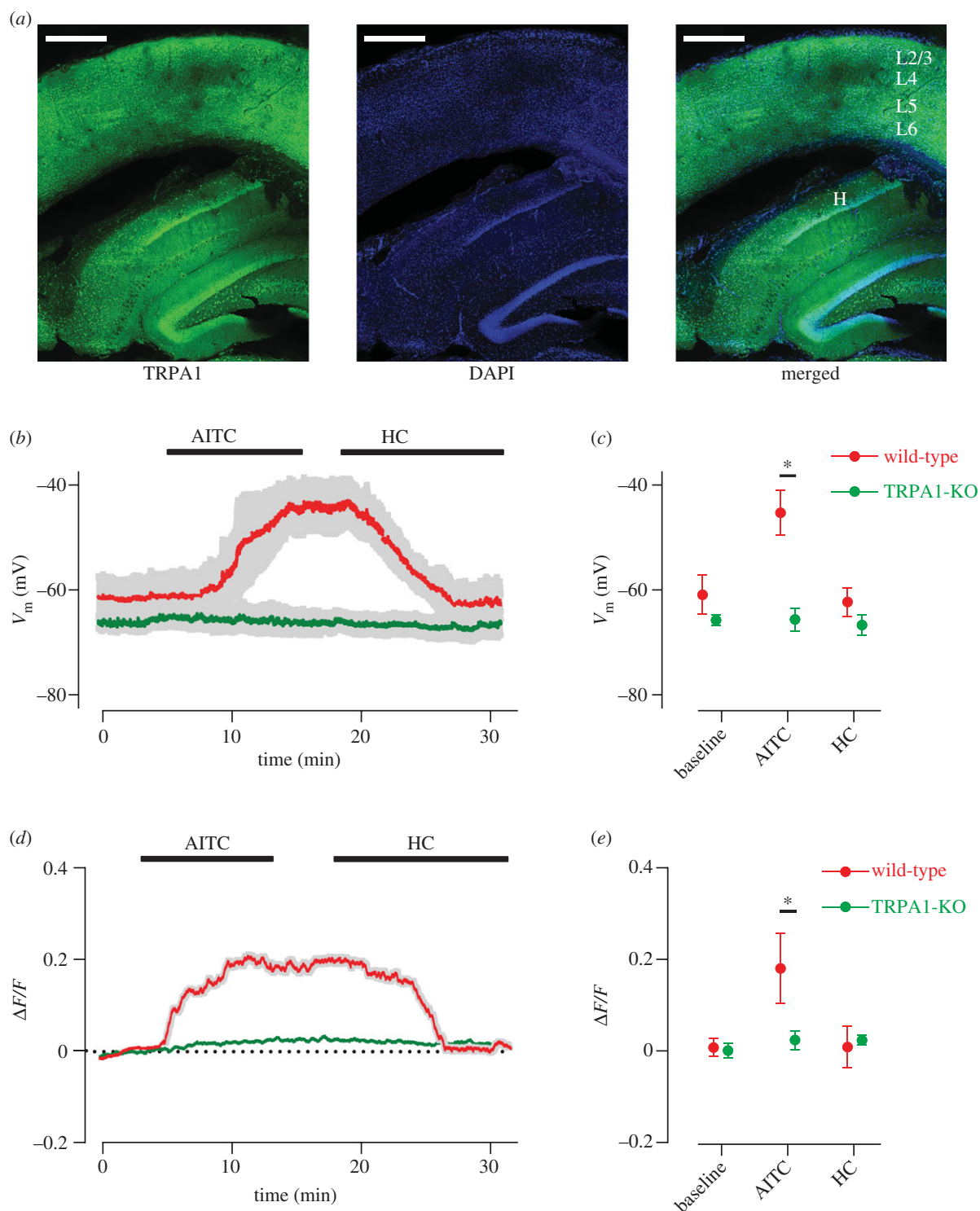


Figure 4. Expression of TRPA1 in mouse cortex and lack of functionality in the knockout. (a) Confocal images of a cortical slice (coronal section) from wild-type mouse capture anti-TRPA1 antibody (green) merged with nuclear staining with DAPI (blue). Scale bar, 500 μm in all panels. (b) Whole-cell recording of L5 pyramidal neurons of wild-type mice (red) reveal depolarization with TRPA1 agonist AITC. The shaded area indicates s.e.m. of V_m across neurons ($n = 3$). By replacing AITC with specific TRPA1 antagonist HC-030031 (HC), the membrane potential returned to its baseline values (hyperpolarized). Similar recording from L5 pyramidal neurons ($n = 3$) of TRPA1-KO mice (green) did not show a significant modulation in response to AITC or HC. (c) The mean V_m values and s.e.m. at each critical time point: at baseline (baseline, 2.5 min); after application of agonist (AITC, 15 min); and after application of antagonist (HC, 27.5 min). $*p < 0.001$, $n = 3$ for each circle. (d) Cortical neurons were loaded with Cal-520. Five minutes after the onset of imaging, AITC was applied to the bath, followed by washing and then by application of HC-030031 (HC). The grey shaded area indicates s.e.m. of $\Delta F/F$ across neurons ($n = 153$ and 156 for wild-type and TRPA1-KO, respectively) recorded in six imaging experiments. (e) $\Delta F/F$ measured at three time points after the onset of imaging: 2.5 min (baseline), 15 min (AITC) and 27.5 min (HC). $\Delta F/F$ is measured over a 1 s duration for each cell and averaged across cells. Error bars indicate s.d. of $\Delta F/F$ across neurons. $*p < 0.001$.

Altogether, these experiments indicate the expression of TRPA1 in rodent somatosensory cortex and demonstrate that optovin can be used to optically control the activity of pyramidal neurons at high spatial and temporal

resolution. The two-photon photoswitching of optovin thus provides a precise method for investigating the physiological and pathological roles of TRPA1 in the mammalian cortex.

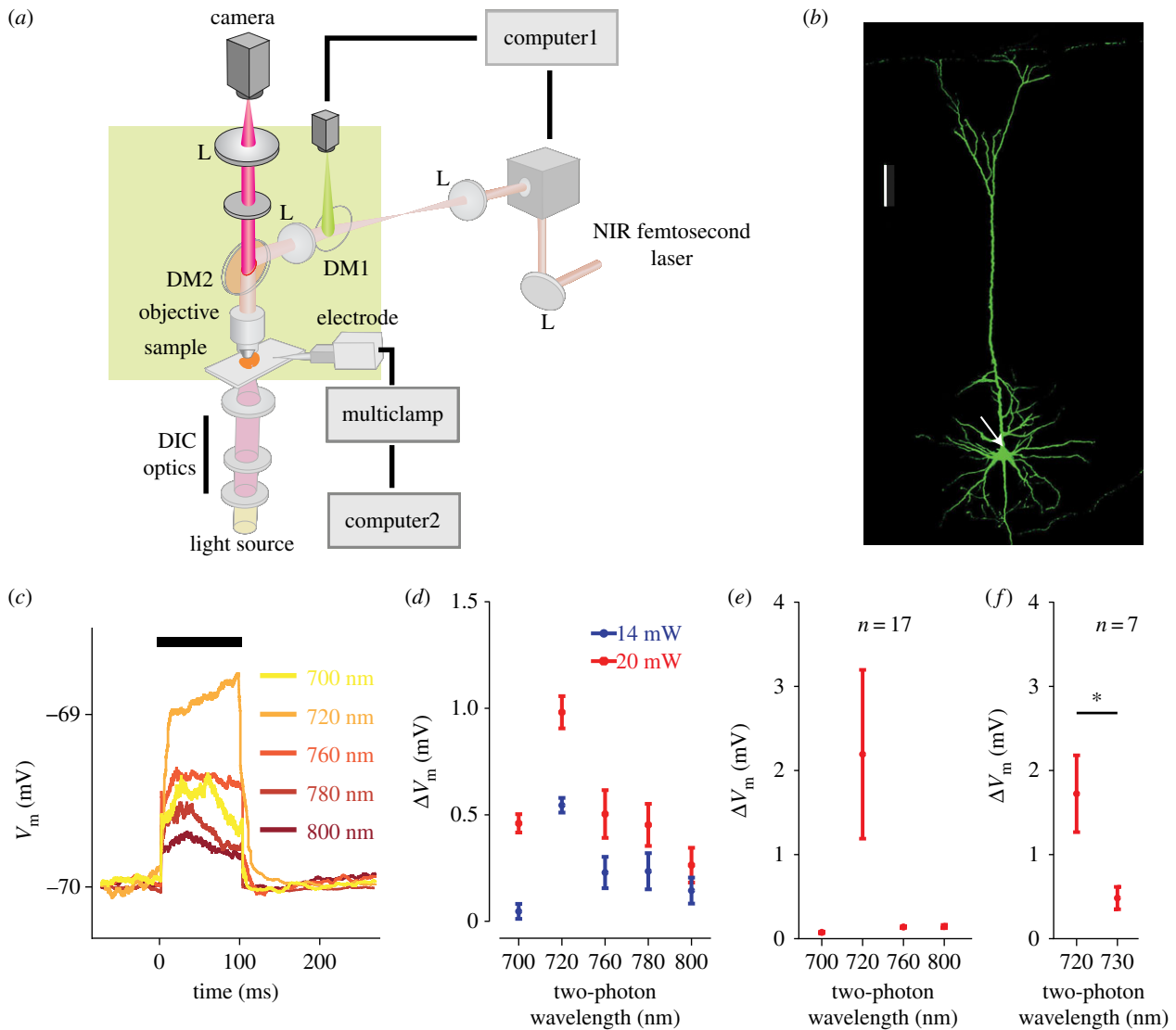


Figure 5. Two-photon photoswitching of optovin-loaded neurons. (a) Schematic of the custom-built two-photon set-up. After transferring the brain slice to the recording chamber, the L5 pyramidal neurons were visualized by applying light through differential interference contrast (DIC) optics using an Olympus BX50WI. This visualization is necessary for targeted whole-cell recording. The dichroic mirror 1 (DM1) reflects fluorescent light ($\lambda < 650$ nm) for two-photon imaging. DM2 passes near-infrared (NIR) light ($\lambda > 900$ nm) for DIC imaging and reflects the lower wavelengths ($\lambda < 900$ nm) for two-photon imaging and optovin photoswitching. The intensity and duration of NIR light is controlled by computer1 via a shutter. A separate computer (computer2) is used for acquisition and analysis of the electrophysiological data. L, lens. (b) Confocal images of a biocytin-loaded L5 pyramidal neuron (green). The arrow indicates the location where the NIR fs-pulsed laser was applied at approximately $1 \mu\text{m}$ diameter. Scale bar, $100 \mu\text{m}$. (c) Two-photon activation of the optovin-loaded neuron shown in (b) at five excitation wavelengths. The neuron was loaded with $3 \mu\text{M}$ optovin. The two-photon excitation beam (20 mW) was applied from 0 to 100 ms (the thick horizontal line). Every line represents the mean V_m across 20 trials of light application. The depolarization was significantly higher at $\lambda = 720$ nm compared with all other wavelengths (all $p < 0.001$). (d) Changes in membrane potential (ΔV_m) of the optovin-loaded neuron (from (b)) in response to two-photon photoswitching. The NIR fs-pulsed laser was applied at each wavelength/intensity combination for a block of 20 trials. These blocks were interleaved in a pseudorandom order and repeated three times to produce 60 trials per condition. Error bars indicate s.e.m. across trials ($n = 60$). The maximum depolarization was observed at $\lambda = 720$ nm ($p < 0.001$ compared with all other wavelengths). (e, f) As in (d) but across L5 pyramidal neurons. Error bars indicate s.e.m. of ΔV_m across neurons ($n = 17$, panel (e); $n = 7$, panel (f)) all loaded with $3 \mu\text{M}$ optovin. * $p < 0.01$.

4. Discussion

To understand a neuronal circuit, a productive approach is to perturb the activity of a specific element, i.e. a dendrite of a neuron or a subpopulation of cells within the circuit, and to quantify the functional consequence of this perturbation. Photostimulation techniques allow perturbation of activity at high spatio-temporal resolution; light has been used to (i) locally uncage neurotransmitters [46], (ii) open photosensitive membrane channels (optogenetics) [47] and (iii) activate synthetic photoswitching molecules which in turn affect endogenous channels [48]. Here, we used optovin

photoswitching for selective targeting of TRPA1 channels that were endogenous to the cortical neurons.

TRPA1 was previously shown to be highly expressed in large cortical vessels and to produce arterial dilatation when activated [41]. Our immunostaining confirmed the prominent presence of TRPA1 in the cortical vasculature. We found that TRPA1 was also expressed in the neurons across layers of the rodent somatosensory cortex, and thus examined its function by application of TRPA1 agonist, AITC, and antagonist, HC-030031. Both two-photon Ca^{2+} imaging and whole-cell electrophysiology revealed TRPA1 modulation of neuronal activity: application of the AITC increased intracellular Ca^{2+}

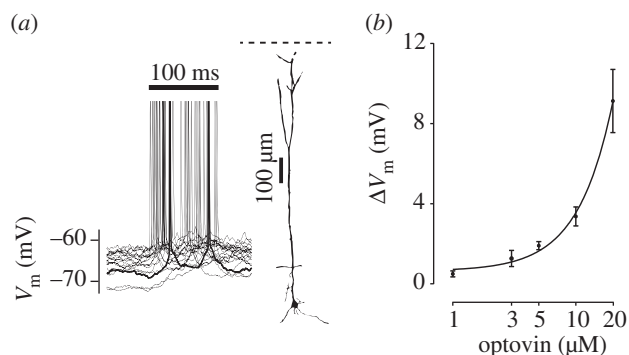


Figure 6. Dose dependency of optovin photoswitching. (a) A sample L5 pyramidal neuron loaded with 20 μM optovin. Laser application ($\lambda = 720$ nm, 20 mW) produced firing of action potentials across all trials. Action potentials are truncated and one of the traces is highlighted in bold. The recorded neuron is histologically reconstructed as L5 pyramidal. The horizontal dashed line indicates cortical surface. (b) The dose–response curve at different optovin concentrations. The curve shows the exponential fit to the data; note the logarithmic scale for optovin concentration. Error bars indicate s.e.m. of ΔV_m across neurons ($n = 5$ at each concentration).

concentration and depolarized the cell membrane, and these effects were blocked by HC-030031, both in the rat cortex and that of wild-type mouse. Importantly, these modulations were absent in the TRPA1-KO mouse. Finally, by targeting TRPA1 through optovin photoswitching, we achieved localized and temporally precise modulation of activity in individual L5 pyramidal neurons. Our results thus extend a previous optovin activation of TRPA1 in the zebrafish [36] to rodents and provide a method to further investigate the role of TRPA1 in the sensory cortex. Previously, violet light, with a wavelength of $\lambda = 385\text{--}405$ nm, was used for single-photon photoswitching of optovin. Light absorption and scattering by the tissue is higher at wavelengths in the visible range [49]. To allow sufficient light penetration in a highly scattering tissue such as the mammalian cortex, an increase in intensity is necessary which can result in cortical damage [50]. We applied an NIR fs-pulsed laser for two-photon excitation at $\lambda = 720$ nm. NIR light has reduced scattering and absorption through cortical tissue resulting in better penetration and a more localized excitation.

The presence of TRPA1 is well established in the peripheral nervous system and a wide range of non-neuronal tissues [7–15]. TRPA1 promotes the process of neurogenic inflammation and enhances the acute or persistent pain sensation [1]. TRPA1 is also thought to be involved in noxious cold sensation [16,51]. TRPA1 is expressed in the inner hair cells [16]. However, despite earlier evidence for its contribution to hearing [16], its functional role is unclear due to the observation of normal hearing in TRPA1-KO mice [45]. In the central nervous system, whole-brain PCR has confirmed the presence of TRPA1 protein but its expression and function has been investigated mostly in the hippocampus and the brain stem [7,14,23]. In hippocampal neurons, TRPA1 is involved in cannabinoid receptor activation [7]. TRPA1 is linked to GABA transport in hippocampal astrocytes, and its activation increases the extracellular GABA concentration, which in turn lowers the efficiency of inhibitory synapses among interneurons [14]. In supraoptic nucleus, TRPA1 agonists produce potentiation of excitatory synaptic inputs in the magnocellular neurosecretory cells possibly through modulation of glutamate release [23]. In the brain stem, TRPA1 is expressed

in the capsaicin-sensitive and capsaicin-insensitive neurons of the nucleus tractus solitarius and is involved in the release of glutamate from these neurons [52]. The common observation across all these studies is an enhanced level of excitability in the circuit by TRPA1 activation.

TRPA1 is widely investigated and better understood in non-mammalian species, where it is associated with several sensations and a range of behavioural responses [7]. In *Caenorhabditis elegans*, TRPA1 is known to mediate the nematode's behavioural response to mechanosensory stimuli [53]. In *Drosophila* (fruit flies), TRPA1 contributes to multiple sensations including nociception, olfaction, noxious cold sensation, negative geotaxis (movement against gravity) and cardiac mechanosensation [54–59]. In snakes, TRPA1 is expressed in the pit organ which is responsible for infrared detection [60].

Beyond its known physiological roles, TRPA1 is implicated in a number of pathological conditions including the generation of asthma, joint oedema, osteoarthritis and skin inflammatory diseases such as acute inflammatory response and allergic contact dermatitis [16–18,37,41,44,61–64]. Similar to its involvement in other tissues and organs, cortical TRPA1 may contribute to physiological functions such as signal processing in sensory cortex and motor behaviours or in developing pathologies such as in Alzheimer's disease [65], brain oedema or oxidative-stress induced neuronal damage.

The recent structural discovery of TRPA1 with electron cryomicroscopy revealed a TRP-domain helix (the transmembrane domain) similar to that of TRPV1 [26]. As well as possessing structural similarities, TRPA1 and TRPV1 are co-expressed in many neuronal and non-neuronal sites [66]. In fact TRPV1 is present in 97% of TRPA1 expressing sensory neurons [51]. It is therefore not surprising that these two channels are involved in similar functions [26,67]. In the peripheral nervous system, both channels contribute to the processing of noxious stimuli including mechanical, thermal and chemical sensations, as well as in pain and neurogenic inflammation [66]. TRPA1 and TRPV1 are also co-expressed in a number of non-neuronal cell types including keratinocytes, endothelial cells and the smooth muscle cells in vessels and have again been implicated in similar pathologies such as joint inflammation and oedema [66]. TRPV1 is expressed in cortex, hippocampus, cerebellum, mesencephalon, hindbrain and olfactory bulb [68]. In the hippocampus and brain stem, TRPA1 and TRPV1 both enhance synaptic glutamate release and are linked to the attenuation of cannabinoid receptors [7,23,52,69,70]. In the human cortex and that of other mammals, TRPV1 is known to be involved in synaptic transmission [70–72]. It is likely that TRPA1 exhibits shared functionality with TRPV1 also in the cortex.

The diverse range of neuronal and non-neuronal cell types that express TRPA1 [66] indicates a highly diverse functional role for this channel. Our findings demonstrate the expression and the functional activation of TRPA1 in rodent cortex. However, these results do not necessarily demonstrate a direct role for this channel in cortical functions such as a contribution to sensory processing or behaviour. It is possible that TRPA1 is activated during pathological conditions such as oedema and brain trauma. This would be consistent with the broad role of TRPA1 in inflammation, infection and immunity observed across a range of tissues. It remains to be investigated how TRPA1 channels interact with other channels in the brain in order to contribute to cortical function and to

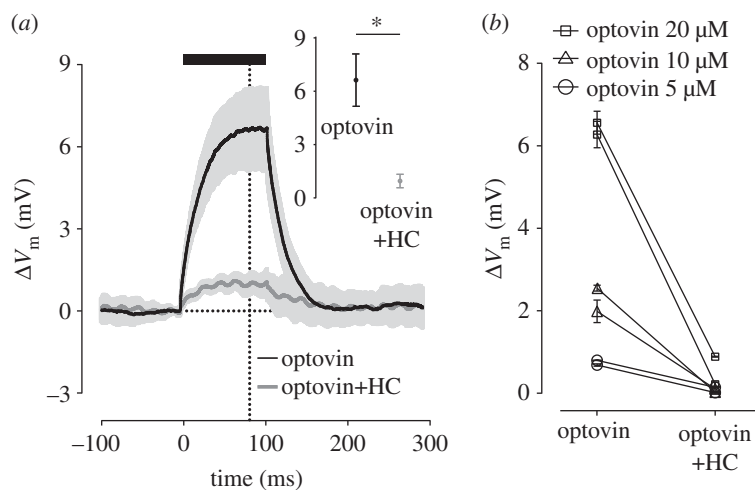


Figure 7. Optovin photoswitching activates neurons through TRPA1 channels. (a) An optovin-loaded neuron is depolarized with light (black). Optovin concentration was 20 μ M. Light application was from 0 to 100 ms as indicated by the thick line. At the end of 20 trials of light application, HC-030031 (HC, 10 μ M) was introduced to the bath and after 10 min of exposure the light stimulation protocol was repeated. Neuronal depolarization to light diminished in the presence of HC-030031 (grey). The inset shows ΔV_m measured 20 ms before the light offset. The shaded area and the error bars (inset) indicate s.e.m. of ΔV_m across trials ($n = 60$). $*p < 0.001$. (b) The effect of HC-030031 is reproduced across neurons ($n = 6$) at three different concentrations of optovin.

pathological conditions. To address these questions future experiments could utilize optovin photoswitching in cortical neurons *in vivo* to specifically target TRPA1 channels at high spatio-temporal precision.

Ethics. All experiments were approved by the Animal Experimentation Ethics Committee at the Australian National University.

Data accessibility. Datasets supporting this article can be found at the central data repository of the Australian National University, see <http://dx.doi.org/10.4225/13/58e1c70673270>.

Authors' contributions. E.K., J.M.C.C., V.R.D. and E.A. conceived and designed the project. E.K. and J.M.C.C. performed the experiments. E.K., J.M.C.C., V.R.D. and E.A. analysed the data. E.K. and E.A.

wrote the manuscript. All authors edited the manuscript and approved the final version. All authors also agreed to be accountable for all aspects of the work in ensuring that questions related to the accuracy or integrity of any part of the work are appropriately investigated and resolved. All persons designated as authors qualify for authorship, and all those who qualify for authorship are listed.

Competing interests. We have no competing interests.

Funding. The experiments were supported by an Australian Research Council (ARC) Discovery Project (DP130101364), an ARC Future Fellowship (E.A.) and the ARC Centre of Excellence for Integrative Brain Function (CE140100007).

Acknowledgements. We thank Stuart Brierley and Grigori Rychkov for valuable discussions and for providing the TRPA1-KO mice.

References

- Julius D. 2013 TRP channels and pain. *Annu. Rev. Cell Dev. Biol.* **29**, 355–384. (doi:10.1146/annurev-cellbio-101011-155833)
- Cortright DN, Krause JE, Broom DC. 2007 TRP channels and pain. *Biochim. Biophys. Acta Mol. Basis Dis.* **1772**, 978–988. (doi:10.1016/j.bbdis.2007.03.003)
- Zayats V, Samad A, Minofar B, Roelofs KE, Stockner T, Ettrich R. 2013 Regulation of the transient receptor potential channel TRPA1 by its N-terminal ankyrin repeat domain. *J. Mol. Model.* **19**, 4689–4700. (doi:10.1007/s00894-012-1505-1)
- Nilius B, Prenen J, Owsianik G. 2011 Irritating channels: the case of TRPA1. *J. Physiol.* **589**, 1543–1549. (doi:10.1113/jphysiol.2010.200717)
- Zurborg S, Yurgionas B, Jira JA, Caspani O, Heppenstall PA. 2007 Direct activation of the ion channel TRPA1 by Ca^{2+} . *Nat. Neurosci.* **10**, 277–279. (doi:10.1038/nn1843)
- Doerner JF, Gisselmann G, Hatt H, Wetzel CH. 2007 Transient receptor potential channel A1 is directly gated by calcium ions. *J. Biol. Chem.* **282**, 13 180–13 189. (doi:10.1074/jbc.M607849200)
- Nilius B, Appendino G, Owsianik G. 2012 The transient receptor potential channel TRPA1: from gene to pathophysiology. *Pflugers Arch. Eur. J. Physiol.* **464**, 425–458. (doi:10.1007/s00424-012-1158-z)
- Nassenstein C, Kwong K, Taylor-Clark T, Kollarik M, Macglashan DM, Braun A, Udem BJ. 2008 Expression and function of the ion channel TRPA1 in vagal afferent nerves innervating mouse lungs. *J. Physiol.* **586**, 1595–1604. (doi:10.1113/jphysiol.2007.148379)
- Doihara H, Nozawa K, Kawabata-Shoda E, Kojima R, Yokoyama T, Ito H. 2009 Molecular cloning and characterization of dog TRPA1 and AITC stimulate the gastrointestinal motility through TRPA1 in conscious dogs. *Eur. J. Pharmacol.* **617**, 124–129. (doi:10.1016/j.ejphar.2009.06.038)
- Earley S, Gonzales AL, Crnich R. 2009 Endothelium-dependent cerebral artery dilation mediated by TRPA1 and Ca^{2+} -activated K^+ channels. *Circ. Res.* **104**, 987–994. (doi:10.1161/CIRCRESAHA.108.189530)
- Nozawa K *et al.* 2009 TRPA1 regulates gastrointestinal motility through serotonin release from enterochromaffin cells. *Proc. Natl Acad. Sci. USA* **106**, 3408–3413. (doi:10.1073/pnas.0805323106)
- Ro JY, Lee JS, Zhang Y. 2009 Activation of TRPV1 and TRPA1 leads to muscle nociception and mechanical hyperalgesia. *Pain* **144**, 270–277. (doi:10.1016/j.pain.2009.04.021)
- Hazari MS, Haykal-Coates N, Winsett DW, Krantz QT, King C, Costa DL, Farraj AK. 2011 TRPA1 and sympathetic activation contribute to increased risk of triggered cardiac arrhythmias in hypertensive rats exposed to diesel exhaust. *Environ. Health Perspect.* **119**, 951–957. (doi:10.1289/ehp.1003200)
- Shigetomi E, Tong X, Kwan KY, Corey DP, Khakh BS. 2012 TRPA1 channels regulate astrocyte resting calcium and inhibitory synapse efficacy through GAT-3. *Nat. Neurosci.* **15**, 70–80. (doi:10.1038/nn.3000)
- Kono T, Kaneko A, Omiya Y, Ohbuchi K, Ohno N, Yamamoto M. 2013 Epithelial transient receptor potential ankyrin 1 (TRPA1)-dependent adrenomedullin upregulates blood flow in rat small intestine. *Am. J. Physiol. Gastrointest. Liver Physiol.* **304**, G428–G436. (doi:10.1152/ajpgi.00356.2012)

16. Corey DP *et al.* 2004 TRPA1 is a candidate for the mechanosensitive transduction channel of vertebrate hair cells. *Nature* **432**, 723–730. (doi:10.1038/nature03066)
17. Anand U *et al.* 2008 TRPA1 receptor localisation in the human peripheral nervous system and functional studies in cultured human and rat sensory neurons. *Neurosci. Lett.* **438**, 221–227. (doi:10.1016/j.neulet.2008.04.007)
18. Brierley SM, Castro J, Harrington AM, Hughes PA, Page AJ, Rychkov GY, Blackshaw LA. 2011 TRPA1 contributes to specific mechanically activated currents and sensory neuron mechanical hypersensitivity. *J. Physiol.* **589**, 3575–3593. (doi:10.1113/jphysiol.2011.206789)
19. Takahashi N, Mizuno Y, Kozai D, Yamamoto S, Kiyonaka S, Shibata T, Uchida K, Mori Y. 2008 Molecular characterization of TRPA1 channel activation by cysteine-reactive inflammatory mediators. *Channels* **2**, 287–298. (doi:10.4161/chan.2.4.6745)
20. Bautista DM, Jordt SE, Nikai T, Tsuruda PR, Read AJ, Poblete J, Yamoah EN, Basbaum AI, Julius D. 2006 TRPA1 mediates the inflammatory actions of environmental irritants and proalgesic agents. *Cell* **124**, 1269–1282. (doi:10.1016/j.cell.2006.02.023)
21. Macpherson LJ, Dubin AE, Evans MJ, Marr F, Schultz PG, Cravatt BF, Patapoutian A. 2007 Noxious compounds activate TRPA1 ion channels through covalent modification of cysteines. *Nature* **445**, 541–545. (doi:10.1038/nature05544)
22. Akopian AN, Ruparel NB, Patwardhan A, Hargreaves KM. 2008 Cannabinoids desensitize capsaicin and mustard oil responses in sensory neurons via TRPA1 activation. *J. Neurosci.* **28**, 1064–1075. (doi:10.1523/JNEUROSCI.1565-06.2008)
23. Yokoyama T, Ohbuchi T, Saito T, Sudo Y, Fujihara H, Minami K, Nagatomo T, Uezono Y, Ueta Y. 2011 Allyl isothiocyanates and cinnamaldehyde potentiate miniature excitatory postsynaptic inputs in the supraoptic nucleus in rats. *Eur. J. Pharmacol.* **655**, 31–37. (doi:10.1016/j.ejphar.2011.01.011)
24. Wang YY, Chang RB, Waters HN, McKemy DD, Liman ER. 2008 The nociceptor ion channel TRPA1 is potentiated and inactivated by permeating calcium ions. *J. Biol. Chem.* **283**, 32 691–32 703. (doi:10.1074/jbc.M803568200)
25. Kim D, Cavanaugh EJ. 2007 Requirement of a soluble intracellular factor for activation of transient receptor potential A1 by pungent chemicals: role of inorganic polyphosphates. *J. Neurosci.* **27**, 6500–6509. (doi:10.1523/JNEUROSCI.0623-07.2007)
26. Paulsen CE, Armache J, Gao Y, Cheng Y, Julius D. 2015 Structure of the TRPA1 ion channel suggests regulatory mechanisms. *Nature* **520**, 511–517. (doi:10.1038/nature14367)
27. Bandell M, Story GM, Hwang SW, Viswanath V, Eid SR, Petrus MJ, Earley TJ, Patapoutian A. 2004 Noxious cold ion channel TRPA1 is activated by pungent compounds and bradykinin. *Neuron* **41**, 849–857. (doi:10.1016/S0896-6273(04)00150-3)
28. Bautista DM, Movahed P, Hinman A, Axelsson HE, Sterner O, Hogestatt ED, Julius D, Jordt S-E, Zygmunt PM. 2005 Pungent products from garlic activate the sensory ion channel TRPA1. *Proc. Natl Acad. Sci. USA* **102**, 12 248–12 252. (doi:10.1073/pnas.0505356102)
29. Jordt S-E, Bautista DM, Chuang H, McKemy DD, Zygmunt PM, Högestätt ED, Meng ID, Julius D. 2004 Mustard oils and cannabinoids excite sensory nerve fibres through the TRP channel ANKTM1. *Nature* **427**, 260–265. (doi:10.1038/nature02282)
30. Takaya J, Mio K, Shiraiishi T, Kurokawa T, Otsuka S, Mori Y, Uesugi M. 2015 A potent and site-selective agonist of TRPA1. *J. Am. Chem. Soc.* **137**, 15 859–15 864. (doi:10.1021/jacs.5b10162)
31. Petrus M, Peier AM, Bandell M, Hwang SW, Huynh T, Olney N, Jegla T, Patapoutian A. 2007 A role of TRPA1 in mechanical hyperalgesia is revealed by pharmacological inhibition. *Mol. Pain* **3**, 40. (doi:10.1186/1744-8069-3-40)
32. Wei H, Chapman H, Saarnilehto M, Kuokkanen K, Koivisto A, Pertovaara A. 2010 Roles of cutaneous versus spinal TRPA1 channels in mechanical hypersensitivity in the diabetic or mustard oil-treated non-diabetic rat. *Neuropharmacology* **58**, 578–584. (doi:10.1016/j.neuropharm.2009.12.001)
33. Wei H, Hämäläinen MM, Saarnilehto M, Koivisto A, Pertovaara A. 2009 Attenuation of mechanical hypersensitivity by an antagonist of the TRPA1 ion channel in diabetic animals. *Anesthesiology* **111**, 147–154. (doi:10.1097/ALN.0b013e3181a1642b)
34. McGaraughty S, Chu KL, Perner RJ, Didomenico S, Kort ME, Kym PR. 2010 TRPA1 modulation of spontaneous and mechanically evoked firing of spinal neurons in uninjured, osteoarthritic, and inflamed rats. *Mol. Pain* **6**, 14. (doi:10.1186/1744-8069-6-14)
35. McNamara CR *et al.* 2007 TRPA1 mediates formalin-induced pain. *Proc. Natl Acad. Sci. USA* **104**, 13 525–13 530. (doi:10.1073/pnas.0705924104)
36. Kokel D *et al.* 2013 Photochemical activation of TRPA1 channels in neurons and animals. *Nat. Chem. Biol.* **9**, 257–263. (doi:10.1038/nchembio.1183)
37. Cordero-Morales JF, Gracheva EO, Julius D. 2011 Cytoplasmic ankyrin repeats of transient receptor potential A1 (TRPA1) dictate sensitivity to thermal and chemical stimuli. *Proc. Natl Acad. Sci. USA* **108**, E1184–E1191. (doi:10.1073/pnas.1114124108)
38. Matta JA, Cornett PM, Miyares RL, Abe K, Sahibzada N, Ahern GP. 2008 General anesthetics activate a nociceptive ion channel to enhance pain and inflammation. *Proc. Natl Acad. Sci. USA* **105**, 8784–8789. (doi:10.1073/pnas.0711038105)
39. Go MA, To M-S, Stricker C, Redman S, Bachor H-A, Stuart GJ, Daria VR. 2013 Four-dimensional multi-site photolysis of caged neurotransmitters. *Front. Cell. Neurosci.* **7**, 231. (doi:10.3389/fncel.2013.00231)
40. Go MA, Stricker C, Redman S, Bachor HA, Daria VR. 2012 Simultaneous multi-site two-photon photostimulation in three dimensions. *J. Biophotonics* **5**, 745–753. (doi:10.1002/jbio.201100101)
41. Sullivan MN *et al.* 2015 Localized TRPA1 channel Ca²⁺ signals stimulated by reactive oxygen species promote cerebral artery dilation. *Sci. Signal.* **8**, ra2. (doi:10.1126/scisignal.2005659)
42. Hinman A, Chuang H-H, Bautista DM, Julius D. 2006 TRP channel activation by reversible covalent modification. *Proc. Natl Acad. Sci. USA* **103**, 19 564–19 568. (doi:10.1073/pnas.0609598103)
43. Gees M *et al.* 2013 Mechanisms of transient receptor potential vanilloid 1 activation and sensitization by allyl isothiocyanate. *Mol. Pharmacol.* **84**, 325–334. (doi:10.1124/mol.113.085548)
44. Bobkov YV, Corey EA, Ache BW. 2011 The pore properties of human nociceptor channel TRPA1 evaluated in single channel recordings. *Biochim. Biophys. Acta Biomembr.* **1808**, 1120–1128. (doi:10.1016/j.bbamem.2010.12.024)
45. Kwan KY, Allchorne AJ, Vollrath MA, Christensen AP, Zhang DS, Woolf CJ, Corey DP. 2006 TRPA1 contributes to cold, mechanical, and chemical nociception but is not essential for hair-cell transduction. *Neuron* **50**, 277–289. (doi:10.1016/j.neuron.2006.03.042)
46. Shoham S, O'Connor DH, Sarkisov DV, Wang SS-H. 2005 Rapid neurotransmitter uncaging in spatially defined patterns. *Nat. Methods* **2**, 837–843. (doi:10.1038/nmeth793)
47. Deisseroth K, Feng G, Majewska AK, Miesenböck G, Ting A, Schnitzer MJ. 2006 Next-generation optical technologies for illuminating genetically targeted brain circuits. *J. Neurosci.* **26**, 10 380–10 386. (doi:10.1523/JNEUROSCI.3863-06.2006)
48. Kramer RH, Fortin DL, Trauner D. 2009 New photochemical tools for controlling neuronal activity. *Curr. Opin. Neurobiol.* **19**, 544–552. (doi:10.1016/j.conb.2009.09.004)
49. Jacques SL. 2013 Optical properties of biological tissues: a review. *Phys. Med. Biol.* **58**, R37–R61. (doi:10.1088/0031-9155/58/11/R37)
50. Kramer RH, Mourof A, Adesnik H. 2013 Optogenetic pharmacology for control of native neuronal signaling proteins. *Nat. Neurosci.* **16**, 816–823. (doi:10.1038/nn.3424)
51. Story GM *et al.* 2003 ANKTM1, a TRP-like channel expressed in nociceptive neurons, is activated by cold temperatures. *Cell* **112**, 819–829. (doi:10.1016/S0092-8674(03)00158-2)
52. Sun B, Bang S-I, Jin Y-H. 2009 Transient receptor potential A1 increase glutamate release on brain stem neurons. *Neuroreport* **20**, 1002–1006. (doi:10.1097/WNR.0b013e32832d2219)
53. Kindt KS, Viswanath V, Macpherson L, Quast K, Hu HZ, Patapoutian A, Schafer WR. 2007 *Caenorhabditis elegans* TRPA-1 functions in mechanosensation. *Nat. Neurosci.* **10**, 568–577. (doi:10.1038/nn1886)
54. Kwon Y, Shim H-S, Wang X, Montell C. 2008 Control of thermotactic behavior via coupling of a TRP channel to a phospholipase C signaling cascade. *Nat. Neurosci.* **11**, 871–873. (doi:10.1038/nn.2170)
55. Sun Y, Liu L, Ben-Shahar Y, Jacobs JS, Eberl DF, Welsh MJ. 2009 TRPA channels distinguish gravity sensing from hearing in Johnston's organ. *Proc. Natl Acad. Sci. USA* **106**, 13 606–13 611. (doi:10.1073/pnas.0906377106)

56. Hwang RY, Stearns NA, Tracey WD. 2012 The ankyrin repeat domain of the TRPA protein Painless is important for thermal nociception but not mechanical nociception. *PLoS ONE* **7**, e30090. (doi:10.1371/journal.pone.0030090)
57. Sénatore S, Reddy VR, Sémériva M, Perrin L, Lalevée N. 2010 Response to mechanical stress is mediated by the TRPA channel Painless in the *Drosophila* heart. *PLoS Genet.* **6**, e1001088. (doi:10.1371/journal.pgen.1001088)
58. Wang K, Guo Y, Wang F, Wang Z. 2011 *Drosophila* TRPA channel Painless inhibits male-male courtship behavior through modulating olfactory sensation. *PLoS ONE* **6**, e25890. (doi:10.1371/journal.pone.0025890)
59. Neely GG *et al.* 2011 TrpA1 regulates thermal nociception in *Drosophila*. *PLoS ONE* **6**, e24343. (doi:10.1371/journal.pone.0024343)
60. Gracheva EO *et al.* 2010 Molecular basis of infrared detection by snakes. *Nature* **464**, 1006–1011. (doi:10.1038/nature08943)
61. Da Costa DSM, Meotti FC, Andrade EL, Leal PC, Motta EM, Calixto JB. 2010 The involvement of the transient receptor potential A1 (TRPA1) in the maintenance of mechanical and cold hyperalgesia in persistent inflammation. *Pain* **148**, 431–437. (doi:10.1016/j.pain.2009.12.002)
62. Liu B *et al.* 2013 TRPA1 controls inflammation and pruritogen responses in allergic contact dermatitis. *FASEB J.* **27**, 3549–3563. (doi:10.1096/fj.13-229948)
63. Wilson S, Nelson AM, Batia L, Morita T, Estandian D, Owens DM, Lumpkin EA, Bautista DM. 2013 The ion channel TRPA1 is required for chronic itch. *J. Neurosci.* **33**, 9283–9294. (doi:10.1016/j.neuron.2011.07.011.Innate)
64. Trevisan G *et al.* 2014 TRPA1 receptor stimulation by hydrogen peroxide is critical to trigger hyperalgesia and inflammation in a model of acute gout. *Free Radic. Biol. Med.* **72**, 200–209. (doi:10.1016/j.freeradbiomed.2014.04.021)
65. Lee K-I, Lee H-T, Lin H-C, Tsay H-J, Tsai F-C, Shyue S-K, Lee T-S. 2016 Role of transient receptor potential ankyrin 1 channels in Alzheimer's disease. *J. Neuroinflammation* **13**, 92. (doi:10.1186/s12974-016-0557-z)
66. Fernandes ES, Fernandes MA, Keeble JE. 2012 The functions of TRPA1 and TRPV1: moving away from sensory nerves. *Br. J. Pharmacol.* **166**, 510–521. (doi:10.1111/j.1476-5381.2012.01851.x)
67. Brewster MSJ, Gaudet R. 2015 How the TRPA1 receptor transmits painful stimuli: Inner workings revealed by electron cryomicroscopy. *BioEssays* **37**, 1184–1192. (doi:10.1002/bies.201500085)
68. Tóth A, Boczán J, Kedei N, Lizanecz E, Bagi Z, Papp Z, Edes I, Csiba L, Blumberg PM. 2005 Expression and distribution of vanilloid receptor 1 (TRPV1) in the adult rat brain. *Brain Res. Mol. Brain Res.* **135**, 162–168. (doi:10.1016/j.molbrainres.2004.12.003)
69. Ross R. 2003 Anandamide and vanilloid TRPV1 receptors. *Br. J. Pharmacol.* **140**, 790–801. (doi:10.1038/sj.bjp.0705467)
70. Peters JH, McDougall SJ, Fawley JA, Smith SM, Andresen MC. 2010 Primary afferent activation of thermosensitive TRPV1 triggers asynchronous glutamate release at central neurons. *Neuron* **65**, 657–669. (doi:10.1016/j.neuron.2010.02.017)
71. Shoudai K, Peters JH, McDougall SJ, Fawley JA, Andresen MC. 2010 Thermally active TRPV1 tonically drives central spontaneous glutamate release. *J. Neurosci.* **30**, 14 470–14 475. (doi:10.1523/JNEUROSCI.2557-10.2010)
72. Mori F *et al.* 2012 TRPV1 channels regulate cortical excitability in humans. *J. Neurosci.* **32**, 873–879. (doi:10.1523/JNEUROSCI.2531-11.2012)